Special Collection

Design, Synthesis and Evaluation of 2,4-Diaminoquinazoline Derivatives as Potential Tubulin Polymerization Inhibitors

Frida S. Herrera-Vázquez,[a] Félix Matadamas-Martínez,[a, b] Rodrigo Aguayo-Ortiz,[c, d] Laura Dominguez,[c] Teresa Ramírez-Apan,[e] Lilián Yépez-Mulia,*[b] and Francisco Hernández-Luis*[a]

Microtubules are highly dynamic polymers composed of α- and β-tubulin proteins that have been shown to be potential therapeutic targets for the development of anticancer drugs. Currently, a wide variety of chemically diverse agents that bind to β-tubulin have been reported. Nocodazole (NZ) and colchicine (COL) are well-known tubulin-depolymerizing agents that have close binding sites in the β-tubulin. In this study, we designed and synthesized a set of nine 2,4-diaminoquinazoline derivatives that could occupy both NZ and COL binding sites. The synthesized compounds were evaluated for their antiproliferative activities against five cancer cell lines (PC-3, HCT-15, MCF-7, MDA-MB-231, and SK-LU-1), a noncancerous one (COS-7), and peripheral blood mononuclear cells (PBMC). The effect of compounds **4e** and **4i** on tubulin organization and polymerization was analyzed on the SK-LU-1 cell line by indirect immunofluorescence, western blotting, and tubulin polymerization assays. Our results demonstrated that both compounds exert their antiproliferative activity by inhibiting tubulin polymerization. Finally, a possible binding pose of **4i** in the NZ/COL binding site was determined by using molecular docking and molecular dynamics (MD) approaches. To our knowledge, this is the first report of non-N-substituted 2,4-diaminoquinazoline derivatives with the ability to inhibit tubulin polymerization.

Introduction

Microtubules are key cytoskeletal components involved in different cellular processes, such as signalization, shape maintenance, motility, intracellular transport, and mitosis.[1] These highly dynamic polymers are composed of α- and β-tubulin heterodimers assembled in a head-to-tail arrangement to form a hollow cylindrical structure.[2] Due to their participation in key functions linked with cell survival, microtubules have shown to be a suitable target for the treatment of cancer, parasitic, and neurodegenerative diseases.[3–6]

Several tubulin-depolymerizing agents (TDAs) and tubulin-stabilizing agents (TSAs) with diverse chemical structures have been reported to date, of which more than 50 have been co-crystallized with tubulin hetero-tetramers within the past 10 years.[7] Except for pironetin, all these agents bind to the β-tubulin and trigger cell mitotic catastrophe or elongation of the microtubule.[8] Five different binding sites in β-tubulin have been identified, the colchicine (COL) site being one of the most studied as it can bind a wide range of small chemically diverse molecules (Figure 1A).[9] COL is a known TDA that promotes microtubule depolymerization by favoring the curved conformation of the protofilaments.[10] The binding site of the potent TDA nocodazole (NZ) was recently solved near COL site, occupying the same pocket as mivobulin (MIV).[11,12] Interestingly, the NZ site varies in sequence between tubulin isoforms, allowing the design of more selective molecules. A previous study performed by our research group showed that compounds that bind to NZ site have a low probability of being hematotoxic due to the inability to interact with the highly expressed βVI tubulin isoform in blood cells.[13] The latter increased our interest in designing molecules that bind to the NZ binding site.

According to our previous pharmacophore hypothesis and the recent crystallographic data, the following pharmacophoric features should be addressed by a molecule to bind in the NZ site: an aromatic scaffold, an H-bond acceptor, two nearby H-

[a] F. S. Herrera-Vázquez, Dr. F. Matadamas-Martínez, Prof. F. Hernández-Luis
Departamento de Farmacia
Universidad Nacional Autónoma de México
Mexico City 04510 (Mexico)
E-mail: franher@unam.mx
[b] Dr. F. Matadamas-Martínez, Prof. L. Yépez-Mulia
Unidad Médica de Alta Especialidad-Hospital de Pediatría
Centro Médico Nacional Siglo XXI
Instituto Mexicano del Seguro Social
Mexico City 06720 (Mexico)
E-mail: lilianyepez@yahoo.com
[c] Dr. R. Aguayo-Ortiz, Prof. L. Dominguez
Departamento de Fisicoquímica
Universidad Nacional Autónoma de México
Mexico City 04510 (Mexico)
[d] Dr. R. Aguayo-Ortiz
Department of Internal Medicine
Division of Cardiovascular Medicine
University of Michigan
Ann Arbor, MI 48109 (USA)
[e] T. Ramírez-Apan
Instituto de Química
Universidad Nacional Autónoma de México
Mexico City 04510 (Mexico)

Supporting information for this article is available on the WWW under https://doi.org/10.1002/cmdc.202000185

This article belongs to the Special Collection "BrazMedChem 2019: Medicinal Chemistry in Latin America"

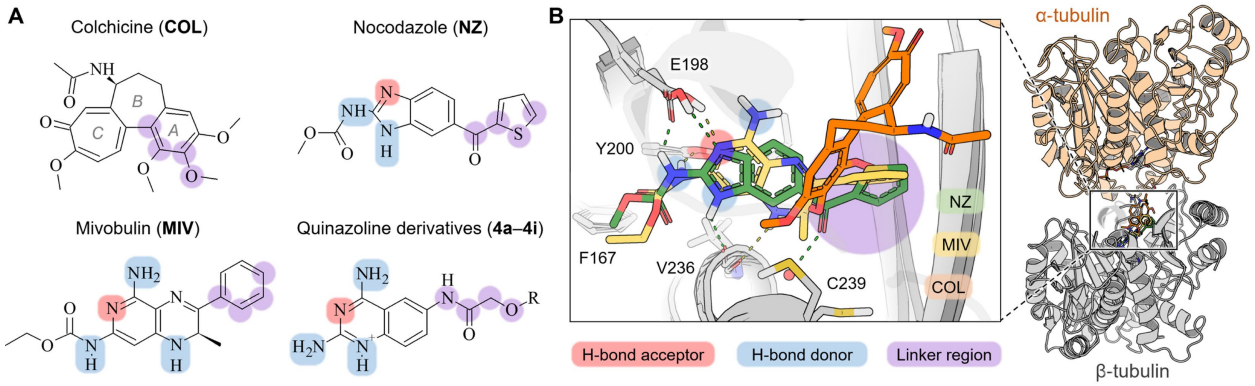

Figure 1. A) Chemical structure of the tubulin-depolymerizing agents (TDAs): colchicine, nocodazole, and mivobulin, as well as the proposed quinazoline derivatives. The structural features for enhancing β-tubulin affinity and conserving tubulin depolymerizing activity are: H-bond acceptor (red), H-bond donor (blue), and linker region (violet). B) Depiction of NZ (green, PDB ID: 5CA1[12]), COL (orange, PDB ID: 4O2B[16]), and MIV (yellow, PDB ID: 3 N2G[11]) binding poses in the β-tubulin.

bond donors, and a distal aromatic substituent (Figure 1B).[13] The protonated state of E198 residue favors the H-bond interaction with the scaffold fused nitrogen, while the H-bond donor groups interact with either E198 or Y200 side chains and with the main chain carbonyl of V236.[14,15] Additionally, the primary amine in the C5 position of MIV could favor its interaction with E198. Initially, the carbamate group was thought to be indispensable for binding due to its interaction with the N165 residue; however, the absence of this interaction in other ligands that bind to this site suggests otherwise.[12] Finally, the aromatic substituents located at the C6 and C3 positions of the NZ and MIV, respectively, are oriented towards the COL binding site.

The quinazoline moiety is considered a privileged structure in medicinal chemistry due to its broad range of biological activities and drug-like properties.[17] Most of the compounds containing this scaffold have shown therapeutic potential as anticancer agents, some of which have been approved by the Food and Drug Administration (FDA) for clinical use (e.g., gefitinib).[18,19] Our research group recently reported a set of quinazoline-2,4,6-triamine derivatives with acceptable cytotoxic activity against five different cancer cell lines.[20] As the quinazoline-2,4,6-triamine moiety possesses pharmacophoric features similar to those of MIV, we hypothesized that this structure could bind to the NZ binding site in the β-tubulin. It is worth mentioning that the scaffold was selected because the N1 nitrogen is more likely to be protonated within the binding site to interact with V236 as it is more basic ($pK_a \approx 7.96$) than that of 2,4-aminopteridine ($pK_a \approx 5.32$) and pyrido[2,3-d]pyrimidine-2,4-diamine ($pK_a \approx 6.62$) itself.[21] Moreover, this proton at position N1 plays a key role in the interaction with other anticancer targets (e.g., G9a[22] and dihydrofolate reductase[23]). Based on the pharmacophoric information, we designed a synthetically accessible four-atom semiflexible linker that could facilitate the R group orientation towards the COL binding site. It is known that the presence of H-bond acceptor/donor groups in this position could favor the interaction of the molecule with structural water molecules.[24] Finally, we replaced the R group with phenyl and quinoline moieties to occupy the sites of the cycloheptane (B ring) and/or the tropolone (C ring) rings of COL. Some positions of these aromatic structures were further substituted with low hydrophilic and hydrophobic groups that could contribute to the interaction with this hydrophobic site. Like tirbanibulin, it is intended that the designed compounds occupy NZ and COL binding sites to promote microtubule destabilization.[25,26]

In this explorative work, we synthesized a set of nine 2,4-diaminoquinazoline derivatives containing phenyl- and quinolinyl-substituted linkers at sixth position (C6). The antiproliferative activity of these compounds was determined in different types of cancer cell lines (PC-3, HCT-15, MCF-7, MDA-MB-231, and SK-LU-1), a noncancerous cell line (COS-7) and peripheral blood mononuclear cells (PBMC). The effect of the most potent compounds on tubulin organization and polymerization was analyzed using indirect immunofluorescence (IFA), western blotting, and tubulin polymerization assays. Finally, we performed molecular docking and molecular dynamics (MD) simulations to address the most probable binding pose of the most potent compound in the NZ and COL binding sites.

Chemistry

Nine 2,4-diaminoquinazoline derivatives (**4a**–**4i**) were synthesized according to the reactions shown in Scheme 1. First, a chloroacetyl chloride solution was dropwise added to a stirred mixture of 5-amino-2-fluorobenzonitrile (**1**) and sodium bicarbonate in acetone to obtain compound **2**. Compound **2** was subsequently added to the mixture of the appropriately substituted phenol or 8-hydroxiquinoline and potassium carbonate in dimethylformamide (DMF) to accomplish the synthesis of compounds **3a**–**3i**. These latter compounds were obtained as solids with acute melting points and spectroscopic data (see Experimental Section). Lastly, cyclocondensation of the isolated reaction intermediates **3a**–**3i** with guanidine carbonate and diisopropylethylamine (DIPEA) were carried out

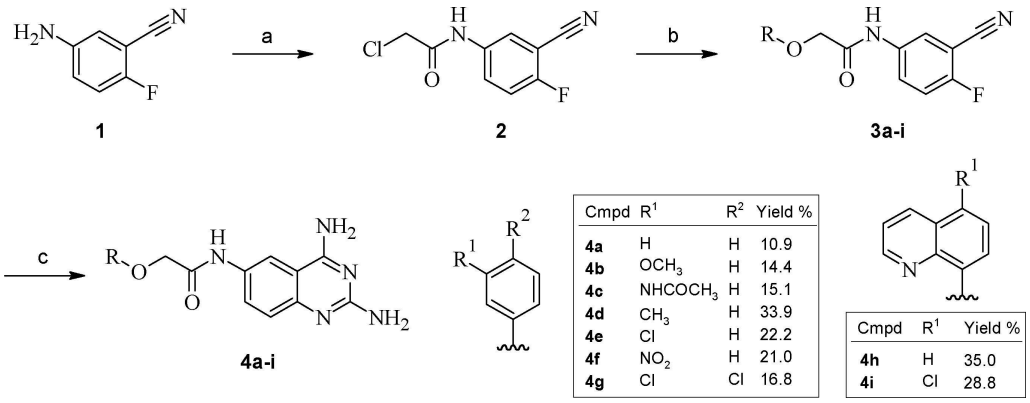

Scheme 1. Synthesis of quinazoline derivatives **4a**–**4i**. a) $ClCH_2COCl$, $NaHCO_3$, CH_3COCH_3, RT, 2.5 h; (b) substituted phenol and 8-hydroxiquinolyl compounds, K_2CO_3, DMF, 85 °C, 7 h; (c) $(C(NH_2)_3)_2CO_3$, DIPEA, DMF, MW, 145 °C, 850 W, 1.5 to 2.5 h. The tables show the R1 and R2 substituents and the overall reaction yield of each compound (Cmpd).

to obtain the final quinazoline derivatives. Spectrometric and spectroscopic data agree with the presented structures (see the Experimental Section and Figures S1 to S27 in the Supporting Information).

Results and Discussion

The synthesized compounds were evaluated against five different types of cancer cell line (PC-3, HCT-15, MCF-7, MDA-MB-231, and SK-LU-1) to determine their antiproliferative activity at 25 μM (Table 1). In addition, compounds cytotoxicity was evaluated on the benign COS-7 cell line and human PBMC. Compounds **4b**, **4d**, **4e** and **4i** showed the highest antiproliferative activity against all the cancer cell lines tested. In particular, compounds **4e** and **4i** showed the highest antiproliferative activity. These compounds and gefitinib, a known anticancer compound comprising a quinazoline moiety, were cytotoxic against COS-7 cells. Compounds **4f** and **4g** did not show activity against MCF-7 and MDA-MB-231 cells and in general terms they showed lower antiproliferative activity than **4b**, **4d**, **4e** and **4i**. Finally, compounds **4a**, **4c**, and **4h**, had the lowest antiproliferative activity against cell lines.

The antiproliferative results showed that the substitution of the phenyl group (**4b**, **4d** to **4f**) increases the activity against the tested cell lines when compared to the nonsubstituted form (**4a**). Nevertheless, a drop in the activity was observed when the *meta* position of the phenyl was substituted by an acetamide group (**4c**). Compound **4e** structure was further optimized by adding chlorine at position 4 (**4g**), but no significant changes in the antiproliferative activity were observed.

When using the quinoline ring in compound **4h**, it was expected that this could keep a similar antiproliferative activity compared to **4d** and **4e**. However, the compound showed a much lower activity, like that of the unsubstituted phenyl group. Interestingly, a significant increase in antiproliferative activity was observed in the six cell lines when replacing the hydrogen at position 5 of the quinoline with a chlorine atom (**4i**).

In addition, IC_{50} determination of compounds that exhibited the best activity against MDA-MB-231 and SK-LU-1 was performed (Table 1). NZ and COL as TDAs, and gefitinib as an

Table 1. Antiproliferative activity, half inhibitory concentration, and 50% cytotoxicity concentration of 2,4-diaminoquinazoline derivatives and reference compounds.

Compound	Antiproliferative activity [%][a]						IC_{50} [μM)]		CC_{50} [μM]
	PC-3	HCT-15	MCF-7	MDA-MB-231	SK-LU-1	COS-7	MDA-MB-231	SK-LU-1	PBMC
4a	38.9 ± 2.7	25.8 ± 4.2	16.1 ± 2.0	10.3 ± 1.8	< 5.0	15.7 ± 1.8	n.d.	n.d.	n.d.
4b	72.1 ± 1.9	70.5 ± 3.5	80.9 ± 3.0	80.7 ± 1.9	76.5 ± 2.1	43.5 ± 3.9	15.6 ± 1.6	25.4 ± 2.3	n.d.
4c	25.9 ± 3.2	23.8 ± 2.5	10.4 ± 2.3	7.3 ± 0.8	< 5.0	13.2 ± 0.9	n.d.	n.d.	n.d.
4d	70.6 ± 1.6	85.0 ± 2.6	81.9 ± 2.4	91.4 ± 2.3	81.2 ± 2.7	75.4 ± 1.7	10.7 ± 1.4	8.6 ± 0.7	254.95
4e	100.0	100.0	100.0	100.0	100.0	100.0	10.8 ± 1.4	8.2 ± 0.1	200.10
4f	72.4 ± 1.9	78.9 ± 2.2	25.5 ± 3.0	65.3 ± 2.2	60.6 ± 1.6	45.6 ± 2.4	23.3 ± 1.2	36.6 ± 2.9	n.d.
4g	65.4 ± 3.5	82.9 ± 2.7	81.7 ± 3.0	40.4 ± 4.5	65.9 ± 3.0	67.3 ± 2.3	n.d.	n.d.	n.d.
4h	12.6 ± 1.5	30.2 ± 3.5	31.5 ± 4.9	27.4 ± 2.7	14.6 ± 1.4	< 5.0	n.d.	n.d.	n.d.
4i	100.0	100.0	100.0	100.0	100.0	100.0	4.8 ± 0.2	5.0 ± 0.2	227.06
NZ	n.d.	n.d.	n.d.	n.d.	n.d.	n.d.	0.21 ± 0.004	0.023 ± 0.001	405.13
COL	n.d.	n.d.	n.d.	n.d.	n.d.	n.d.	0.03 ± 0.003	0.007 ± 0.001	567.98
gefitinib	n.d.	n.d.	n.d.	n.d.	n.d.	64.3 ± 3.2	28.0 ± 2.6	16.3 ± 1.7	n.d.

[a] Quinazoline derivatives **4a**–**4d**, **4f**–**4i**, and gefitinib were evaluated at 25 μM. n.d.: not determined.

anticancer drug, were included as reference controls. Compounds **4d**, **4e** and **4i** showed the lowest IC_{50} value of the quinazoline derivatives; they were lower than gefitinib but higher than the reference compounds, NZ and COL. Therefore, although our compounds are not as potent as the reference TDAs, they have significant antiproliferative activity in comparison to gefitinib, an FDA-approved drug used for the treatment of non-small-cell lung cancer.[27] As our quinazoline derivatives were designed based on the NZ binding site, it was expected that these molecules were less cytotoxic to PBMC. Our results demonstrated that these quinazoline derivatives were more potent against cancer cell lines than to PBMC of healthy patients. However, these derivatives were shown to be more cytotoxic to PBMC than NZ and COL.

The effect of compounds with the highest antiproliferative activity (**4d**, **4e**, and **4i**) on the cellular microtubule network of SK-LU-1 cells was examined by IFA. Paclitaxel (PTX), NZ and COL were employed as reference compounds and DMSO as negative control (Ctrl). In the absence of drug treatment, microtubules displayed a normal distribution and arrangement in SK-LU-1 cells (Figure 2). PTX, a well-known TSA, promoted the cell mitotic arrest, leading to spherical cell shape and condensation of mitotic spindles, in agreement with other studies.[28] NZ treatment induced rounded-shaped cells with the absence of typical mitotic spindles, while treatment with COL led to asymmetrically shaped cells with an increase in the nucleus size and the absence of typical mitotic spindles. Compounds **4e** and **4i** behaved like TDAs, both promoted morphological alterations in SK-LU-1 cells such as multinucleation, increase in the nucleus size and chromosome condensation, indicative features of mitotic catastrophe.[29,30] Cells treated with **4d** presented different morphological features to those observed with PTX and TDAs, thus suggesting that this compound might have a mechanism of action other than tubulin polymerization inhibition. It is worth mentioning that compounds **4e** and **4d** were evaluated at different concentrations, including their IC_{50} values, in order to demonstrate in more detail their effect on SK-LU-1 microtubules. However, even at three-fold higher concentration, compound **4d** did not show any alterations in microtubules as observed at much lower concentrations with compound **4e**. Regarding compound **4i**, even at the half of its IC_{50} value (2.5 μM), its effect on SK-LU-1 microtubules network was observed (Figure 2). Therefore, we focused our attention on compounds **4e** and **4i**.

IFA showed that compounds **4e** and **4i** induce alterations in the microtubule network. Similar alterations in microtubule dynamics are often related to modifications in the tubulin polymerization as a result of the direct interaction of the compounds with the β-tubulin protein.[31] In order to identify the mechanism by which **4e** and **4i** compounds affect the stability of the microtubules, soluble and polymerized tubulin protein obtained from treated SK-LU-1 cells were analyzed by western blotting (Figure 3A). PTX and NZ were included as positive controls and DMSO (0.01%) as negative control.

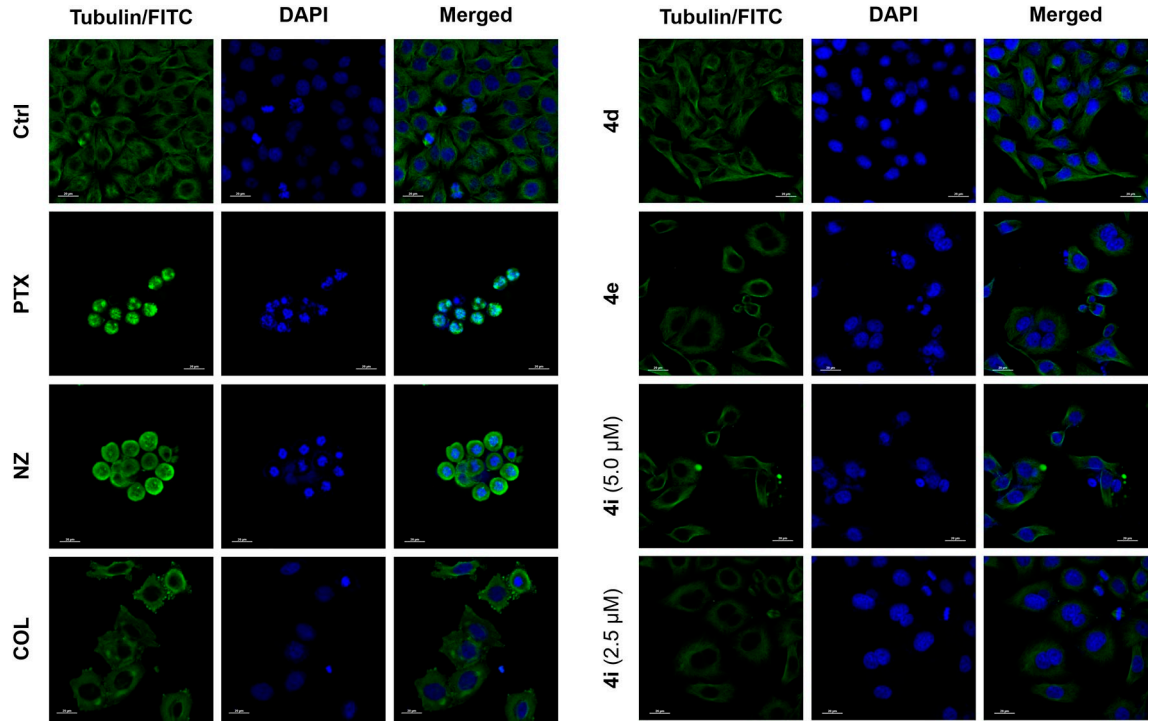

Figure 2. Indirect Immunofluorescence SK-LU-1 cells treated with **4d**, **4e** and **4i**. Cells were treated with DMSO at 0.01% (Ctrl), PTX (0.08 μM), NZ (0.16 μM), COL (0.30 μM), **4d** (25.0 μM), **4e** (12.5 μM), and **4i** (5.0 and 2.5 μM) for 24 h. The cell samples were incubated with anti-β-tubulin antibody (1:1000) and anti-mouse IgG-FITC (1:1000) as secondary antibody. The nuclear DNA was counterstained with 4,6-diamidino-2-phenylindole (DAPI). β-tubulin is stained in green, DNA in blue. Panels show the microtubules stained with FITC (first column), DAPI (second column), and these columns merged (third column). Samples were visualized by confocal microscopy. Scale bars: 20 μm.

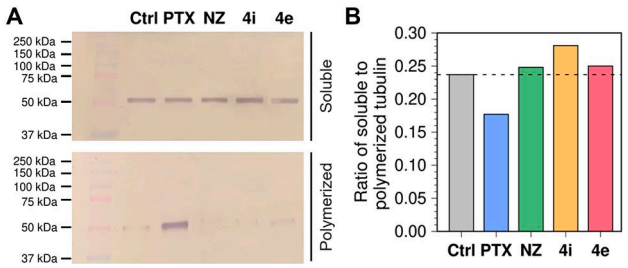

Figure 3. A) Soluble and polymerized tubulin fractions of control cells and samples treated with PTX (0.08 μM), NZ (0.16 μM), **4i** (5.00 μM), and **4e** (12.5 μM). B) Ratio of soluble-to-polymerized tubulin of the data depicted in A.

Soluble tubulin was detected in untreated cells as well as in treated cells; however, polymerized tubulin was mainly detected in untreated cells and PTX treated cells. Densitometric analysis of soluble and polymerized tubulin detected in each treatment was performed, and the ratio of soluble to polymerized tubulin fractions was determined for each compound (Figure 3B). As expected, PTX showed a lower ratio of soluble to polymerized tubulin compared to the control due to its stabilizing contribution to the polymerization of tubulin proteins. Meanwhile, NZ and compounds **4e** and **4i** had a higher ratio of soluble to polymerized tubulin in comparison to control and PTX. Compound **4i** showed the highest ratio of soluble to polymerized tubulin. These data suggest that both synthesized compounds exhibit a tubulin polymerization inhibitory activity.

To confirm that **4e** and **4i** behave as TDAs, a tubulin polymerization inhibition assay was carried out employing the kit BK006P manufactured by Cytoskeleton Inc. and following the manufacturer's instructions. This kit uses a purified porcine brain β-tubulin (UniProt: P02554) for the polymerization assay, which has a high sequence identity with human βI (UniProt: P07437, ID: 96.0%) and βIII (UniProt: Q13509, ID: 91.6%) tubulin isoforms overexpressed in breast and lung cancer cell lines.[32] PTX and NZ were also included as reference compounds. Tubulin polymerization curves of control and reference compounds are shown in Figure 4A. NZ (0.16 μM) displayed a significant reduction in the maximum initial velocity (V_{max}) in the growth phase of tubulin polymerization ($V_{max} = 7.25 \pm 0.75$ mOD/min), in comparison to control ($V_{max} = 20.5 \pm 1.5$ mOD/min). Conversely, PTX showed a high V_{max} value ($V_{max} = 50.0 \pm 1.0$ mOD/min) compared to control, due to the initial increase in the polymerization rate. The tubulin polymerization curve of compounds **4e** and **4i** (tested at different concentrations) is presented in Figures 4B and C, respectively. It shows that **4e** at 10 μM has a marginal polymerization inhibitory activity ($V_{max} = 14.5 \pm 0.5$ mOD/min), in comparison to the control. Meanwhile, compound **4i** reduced the tubulin polymerization rate in a concentration-dependent manner. At 10 μM, **4i** ($V_{max} = 4.0 \pm 0.0$ mOD/min) exhibited a similar tubulin polymerization curve to that of NZ at 0.16 μM. Interestingly, at 5 and 2.5 μM, compound **4i** also showed a reduction of the maximum initial velocity ($V_{max} = 11.0 \pm 1.0$ and 13.0 ± 0.0 mOD/min, respectively). Even at lower concentrations, compound **4i** has similar or higher tubulin polymerization inhibitory activity than other TDAs reported in the literature.[31,33–35] It should be mentioned that none of the other synthesized compounds induced significant changes in tubulin polymerization (Figure S28).

Based on our initial hypothesis, compound **4i** could be exerting its polymerization inhibitory activity by binding to the NZ/COL binding site in the β-tubulin. To corroborate the proposed binding mode and interaction profile of **4i** in this binding site, we carried out molecular docking and MD studies at the NZ/COL site using the β-tubulin crystal structure of *Gallus gallus* (PDB ID: 5CA1[12]). It is worth mentioning that *G. gallus* β-tubulin shares high sequence identity with human βI (ID: 95.5%) and βIII (ID: 90.9%) tubulin isoforms overexpressed in breast and lung cancer cell lines.[32] Except for C239, the residues comprising the binding site are highly conserved between the two human isoforms and the *G. gallus*. Furthermore, *Sus barbatus* α-tubulin was replaced in the heterodimer with that of *Sus scrofa* (PDB ID:5yl2[36]) because the orientation of the loop comprising the T179 residue in this last structure is key for the internalization of molecules into COL binding site and to avoid structural clashes.

Figure 5 shows the binding pose of **4i** within the NZ/COL binding site in the β-tubulin and the superposition of co-crystallized MIV, NZ, and COL structures. This binding mode of

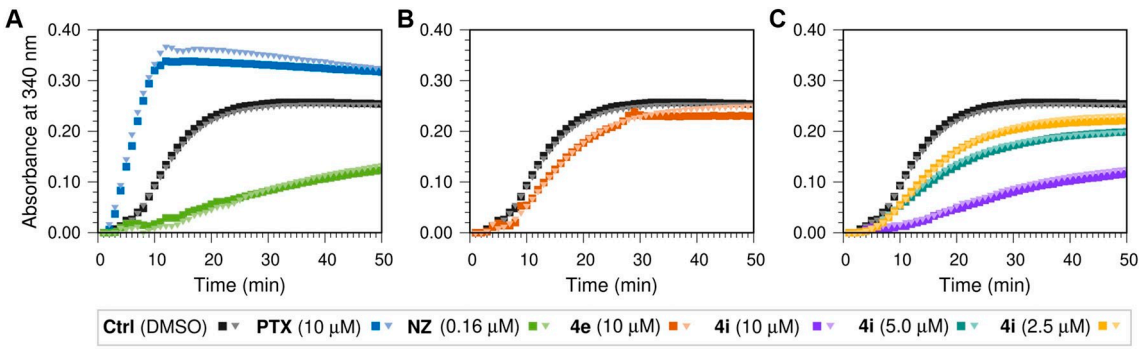

Figure 4. Tubulin polymerization curves of purified porcine brain tubulin in the absence (Ctrl) and presence of A) reference compounds (PTX and NZ), B) **4e**, and C) **4i** at different concentrations. All samples were evaluated in duplicate (square and triangle).

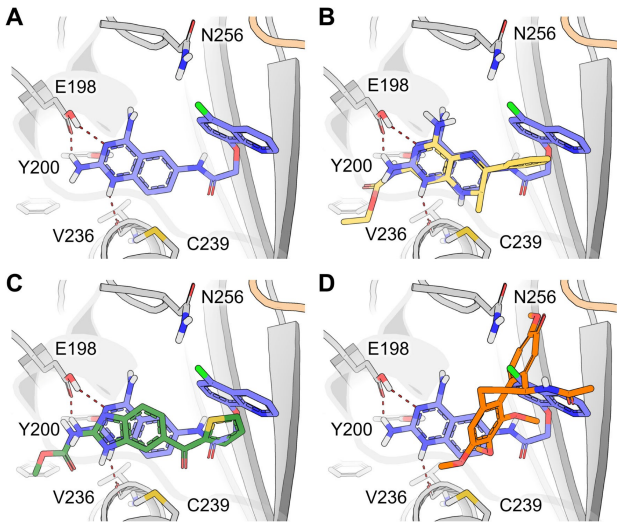

Figure 5. A) Depiction of the **4i** binding pose and intermolecular interactions within the NZ/COL binding site in the β-tubulin of *G. gallus* (PDB ID: 5CA1). Superposition of **4i** (purple) and the co-crystal structures of B) MIV (yellow, PDB ID: 3 N2G), C) NZ (green, PDB ID: 5CA1), and D) COL (orange, PDB ID: 4O2B).

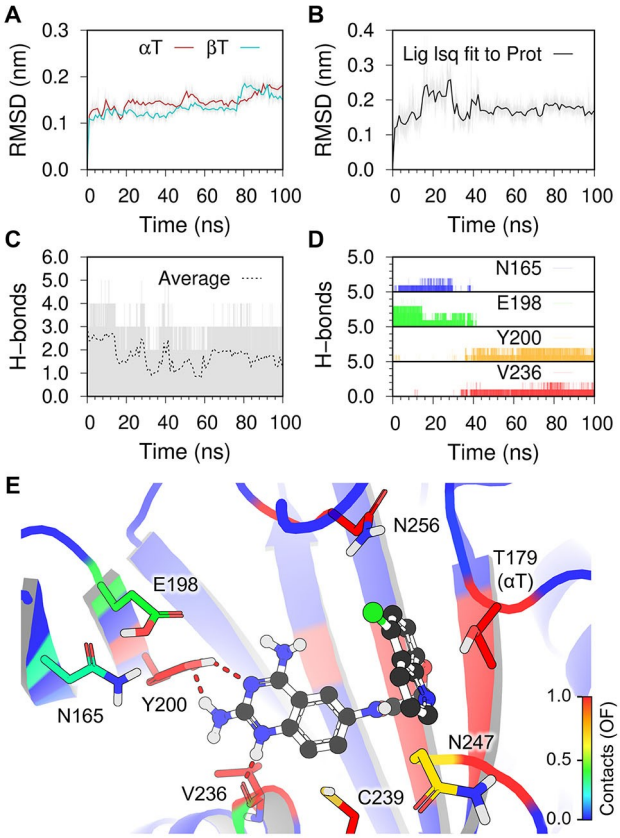

Figure 6. Analysis of the 100 ns MD simulation of α/β-tubulin-**4i** complex. Root-mean-square deviation (RMSD) of (A) α/β-tubulin backbone and (B) **4i** structure calculated after least-square fit to β-tubulin. (C) Average and (D) per amino acid number of H-bonds of **4i** with the NZ/COL binding site through the simulation. (E) Depiction of residues involved in the interaction of **4i** with α/β-tubulin. The color scale shows the residues located within 3.5 Å of the compound with higher (red) to lower (blue) occupancy fraction (OF) values.

4i showed the largest cluster (39 out of 50) and the best-calculated score (−10.70 kcal/mol) according to AutoDock v4.2. The quinazoline derivative formed three key H-bonds in the NZ site with E198 side chain and V236 main chain. Interestingly, the interaction profile of **4i** in the NZ site is consistent with the previously proposed pharmacophore hypotesis.[13] On the other hand, the acetamide group places the quinoline substituent at the COL site, where the chlorine group could form a H-bond with the N256 side chain.

To corroborate the stability of the protein-ligand interaction, we performed a 100 ns atomistic MD simulation of **4i** complexed with the α/β-tubulin heterodimer by using GROMACS 5.1.4 software (Figure 6). The simulation showed that the ligand did not exhibit a significant conformational change in the last 50 ns of simulation (RMSD ≤ 0.2 nm). During this simulation time, the 2,4-diaminoquinazoline derivative formed an average of two H-bonds with the residues that comprise the binding site. These H-bonds were formed mainly with Y200 side chain (44.3%) and V236 main chain (47.2%). Residue–ligand contact analysis showed that quinazoline nucleus interacted only 37.9% of the simulation time with E198, registering a greater number of contacts with Y200 (99.1%) and V236 (99.6%). In addition, it was observed that the quinazoline substituent had several contacts (99.7%) with the T179 residue of the α-tubulin monomer. The latter could promote the spacing between tubulin monomers, thus favoring the curved shape of the protofilament. Like **4i**, compound **4e** had a stable interaction with the NZ site residues; however, this compound formed H-bonds with E198 side chain during 98.7% of the simulation time (Figure S29). Overall, these results suggest that compound **4i** could exert its polymerization inhibitory activity by binding to the NZ/COL binding site and promoting tubulin depolymerization with a mechanism similar to that of MIV, NZ, and COL.

Conclusion

A set of nine 2,4-diaminoquinazoline derivatives (**4a**–**4i**) has been synthesized, and their antiproliferative activity has been tested against the cancer cell lines PC-3, HCT-15, MCF-7, MDA-MB-231, and SK-LU-1. Compounds **4d**, **4e**, and **4i** showed the highest antiproliferative activity against all cell lines tested. In particular, **4e** and **4i** exhibited the highest antiproliferative activity at 25 μM and the lowest IC_{50} values against MDA-MB-231 (10.8 ± 1.4 and 4.8 ± 0.2 μM, respectively) and SK-LU-1 (8.2 ± 0.1 and 5.0 ± 0.2 μM, respectively). It is worth mentioning that these derivatives showed higher antiproliferative activity and lower IC_{50} values than gefitinib. It was observed that the substitution of the H atom at position 5 of the quinoline nucleus with a chlorine group (**4i**) improved the antiproliferative activity of the 2,4-diaminoquinazoline derivatives. In addition, IFA, western blotting, and tubulin polymerization

inhibition assays demonstrated that both **4e** and **4i** alter the microtubule network and inhibit tubulin polymerization. Importantly, **4i** at 10 μM showed a tubulin polymerization curve like that of NZ (0.16 μM). Finally, our molecular docking and molecular dynamics studies suggest that **4i** binds to β-tubulin through 2,4-diaminoquinazoline scaffold interaction with the NZ binding site and 6-substituent orientation within the COL binding site. This study represents an important attempt to understand the tubulin polymerization inhibitory activity of 2,4-diaminoquinazoline derivatives for the treatment of lung and breast cancer. Further structural optimization of the hit compound **4i** will give knowledge about the structural requirements to achieve a better biological activity.

Experimental Section

Chemistry

All reactions were monitored by thin-layer chromatography (TLC). The purification of compounds was carried out by flash chromatography and preparative TLC on 0.2 mm precoated silica gel 60 Sigma-Aldrich (230–400 mesh) and Merck silica gel 60 (F254) plates, respectively. Melting points (mp) were determined on an Electrothermal IA9300 Digital Melting Point Instrument and are uncorrected. Microwave reactions were performed using glassware setup for atmospheric-pressure reactions in an Anthon Parr Microwave Monowave 300®, adapted with an infrared sensor for temperature control. Operating conditions were programmed as follows: 140–145 °C, 850 W, 3 min of ramp and 1.5 to 2.5 h of reaction. ^{1}H and ^{13}C NMR spectra were taken in deuterated dimethyl sulfoxide ([D$_6$] DMSO) at room temperature by using Varian RS 400 and 300 MHz instruments. Chemical shifts are given relative to tetrametylsilane (TMS) as an internal reference. ^{13}C NMR assignments were carried out by 2D NMR experiments (HSQC and HMBC). High-resolution mass spectra (HRMS) were recorded on an AxION-2 TOF MS Perkin Elmer spectrometer *m/z* [% rel. int] coupled with an atmospheric pressure chemical ionization (APCI) source.

General procedure for the preparation of compound (2): The commercially available 5-amino-2-fluorobenzonitrile (5.90 mmol) and sodium bicarbonate (12.00 mmol or 2 equiv.) were dissolved in acetone (15 mL), followed by the dropwise addition of a solution of chloroacetyl chloride under stirring and on ice during 30 min. Afterwards, the stirred reaction was placed at RT during 2 h upon completion, the solution was poured in ice and water. The precipitate formed was filtered and washed continuously in order to reach pH 7, and obtain 2-chloro-*N*-(3-cyano-4-fluorophenyl) acetamide (**2**). Light brown solid; Yield: 98.2%; m.p.: 132.7–133.1 °C; ^{1}H NMR (400 MHz, [D$_6$]DMSO): δ = 10.67 (s, 1H), 8.06 (dd, J_1 = 5.7 Hz, J_2 = 2.7 Hz, 1H), 7.82 (ddd, J_1 = 8.8 Hz, J_2 = 4.7 Hz, J_3 = 2.7 Hz, 1H), 7.47 (t, J = 9.1 Hz, 1H), 4.25 (s, 2H); ^{13}C NMR (400 MHz, [D$_6$]DMSO): δ = 165.18, 160.11, 157.60, 135.95, 126.68, 117.30, 117.09, 100.40, 43.75.

General procedure for the preparation of compounds (3a–3i): To a stirring solution of properly substituted phenol and 8-hydroxiquinoline compounds (2.90 to 5.25 mmol or 1.2 equiv.) and potassium carbonate (4.8 to 8.6 mmol) in anhydrous dimethylformamide (DMF, 15 mL), and after 30 min in RT conditions, compound **2** (2.40 to 7.00 mmol) was slowly added. Subsequently, the mixture was heated up to 85 °C for 6–7 h, this was continuously monitored by TLC. The latter was decanted in ice-water resulting in precipitate, this was removed by vacuum filtration washing it with water until pH 7. The solid was obtained by crystallization (dichloromethane/methanol).

***N*-(3-Cyano-4-fluorophenyl)-2-phenoxyacetamide (3a)**: Light brown solid; Yield: 46.8%; m.p.: 143.9–145.2 °C; ^{1}H NMR (400 MHz, [D$_6$]DMSO): δ = 10.48 (s, 1H), 8.16 (dd, J_1 = 5.5 Hz, J_2 = 2.3 Hz, 1H), 7.95 (ddd, J_1 = 7.4 Hz, J_2 = 4.9 Hz, J_3 = 1.4 Hz, 1H), 7.51 (t, J = 9.1 Hz, 1H), 7.32 (t, J = 7.8 Hz, 2H); 7.02 (dd, J_1 = 7.5, J_2 = 1.3 Hz, 2H), 7.00–6.96 (m, 2H), 4.72 (s, 2H), ^{13}C NMR (400 MHz, [D$_6$]DMSO): δ = 167.42, 159.63, 157.65, 135.47, 131.40, 129.53, 127.11, 121.33, 117.17, 116.97, 114.62, 99.83, 67.02.

***N*-(3-Cyano-4-fluorophenyl)-2-(3-methoxyphenoxy)acetamide (3b)**: Brown solid; Yield: 51.2%; m.p.: 142.3–143.6 °C; ^{1}H NMR (400 MHz, [D$_6$]DMSO): δ = 10.43 (s, 1H), 8.16 (ddd, J_1 = 7.4 Hz, J_2 = 4.9 Hz, J_3 = 1.4 Hz, 1H), 7.96 (dd, J_1 = 4.9 Hz, J_2 = 1.4 Hz, 1H), 7.51 (t, J = 9.0 Hz, 1H), 7.21 (t, J = 8.2 Hz, 1H), 6.68 (d, J = 1.5 Hz, 1H), 6.57 (dt,, J_1 = 7.5 Hz, J_2 = 1.4 Hz, 1H), 6.54 (dt, J_1 = 7.5 Hz, J_2 = 1.5 Hz, 1H), 4.71 (s, 2H), 3.74 (s, 3H); ^{13}C NMR (400 MHz, [D$_6$]DMSO): δ = 175.34, 167.59, 160.55, 160.47, 135.48, 130.85, 130.11, 127.24, 117.25, 117.04, 107.05, 106.78, 101.20, 99.88, 67.11, 55.18.

2-(3-Acetamidophenoxy)-*N*-(3-cyano-4-fluorophenyl)acetamide (3c): Light brown solid; Yield: 48.7%; m.p.: 186.4–188.5 °C; ^{1}H NMR (400 MHz, [D$_6$]DMSO): δ = 9.95 (s, 2H), 8.18–8.06 (m, 1H), 7.68 (dd, J_1 = 4.9 Hz, J_1 = 1.4 Hz, 1H), 7.49 (t, J = 7.4 Hz, 1H), 7.42 (dt, J_1 = 7.5 Hz, J_2 = 1.5 Hz, 1H), 7.37 (t, J = 1.4 Hz, 1H), 7.18 (t, J = 8 .1 Hz, 1H), 6.63 (dt, J_1 = 7.3 Hz, J_2 = 1.5 Hz, 1H), 4.68 (s, 1H), 2.50 (s, 3H); ^{13}C NMR (400 MHz, [D$_6$]DMSO): δ = 168.45, 167.26, 157.96, 153.71, 140.55, 135.64, 129.54 (C-14), 131.20 (C-16), 124.28, 117.24, 117.04, 113.96, 108.94, 100.01, 67.03, 24.13.

***N*-(3-Cyano-4-fluorophenyl)-2-(3-methylphenoxy)acetamide (3d)**: Light brown solid; Yield: 79.3%; m.p.: 174.3–176.1 °C; ^{1}H NMR (400 MHz, [D$_6$]DMSO): δ = 10.44 (s, 1H), 8.16 (ddd, J_1 = 7.4 Hz, J_2 = 4.9 Hz, J_3 = 1.4 Hz, 1H), 7.96 (dd, J_1 = 4.9 Hz, J_2 = 1.4 Hz, 1H), 7.32 (t, J = 7.8 Hz, 1H), 7.19 (t, J = 7.5 Hz, 1H), 6.84 (t, J = 1.4 Hz, 1H), 6.83 (dt, J_1 = 7.5 Hz, J_2 = 1.5 Hz 1H), 6.76 (dt, J_1 = 7.5 Hz, J_2 = 1.4 Hz 1H), 4.69 (s, 2H), 2.28 (s, 3H); ^{13}C NMR (400 MHz, [D$_6$]DMSO): δ = 167.35, 159.67, 157.68, 139.09, 135.54, 129.32, 127.22, 123.72, 117.24, 117.03, 115.49, 113.94, 99.86, 66.98, 21.14.

2-(3-Chlorophenoxy)-*N*-(3-cyano-4-fluorophenyl)acetamide (3e): Light brown solid; Yield: 60.4%; m.p.: 198.6–200.1 °C; ^{1}H NMR (400 MHz, [D$_6$]DMSO): δ = 9.77 (s, 1H), 8.03–7.97 (m, 1H), 7.67 (dd, J_1 = 4.9 Hz, J_2 = 1.4 Hz, 1H), 7.32 (t, J = 7.7 Hz, 1H), 7.22 (t, J = 7.5 Hz, 1H), 7.01 (t, J = 1.4 Hz, 1H), 6.98 (dt, J_1 = 7.5 Hz, J_2 = 1.5 Hz, 1H), 6.84 (dt, J_1 = 7.5 Hz, J_2 = 1.4 Hz, 1H), 4.81 (s, 2H); ^{13}C NMR (400 MHz, [D$_6$] DMSO): δ = 170.99, 160.43, 158.90, 137.11, 134.06, 131.77, 131.19, 130.55, 124.85, 121.51, 117.42, 116.16, 114.12, 93.83, 67.10.

***N*-(3-Cyano-4-fluorophenyl)-2-(3-nitrophenoxy)acetamide (3f)**: Light brown solid; Yield: 53.1%; m.p.: 167.2–168.1 °C; ^{1}H NMR (400 MHz, [D$_6$]DMSO): δ = 10.43 (s, 1H), 7.97–7.87 (m, 1H), 7.85 (t, J = 1.4 Hz, 1H), 7.83 (dt, J_1 = 7.5 Hz, J_2 = 1.4 Hz, 1H), 7.66 (dd, J_1 = 5.0 Hz, J_2 = 1.5 Hz, 1H), 7.51 (t, J = 9.1 Hz, 1H), 7.30 (t, J = 8.4 Hz, 1H), 6.60–6.56 (m, 1H), 4.71 (s, 2H); ^{13}C NMR (400 MHz, [D$_6$]DMSO): δ = 167.15, 160.88, 160.08, 157.14, 135.44, 130.15, 127.21, 127.12, 123.72, 119.25, 117.18, 116.98, 113.87, 99.84, 67.13.

***N*-(3-Cyano-4-fluorophenyl)-2-(3,4-dichlorophenoxy)acetamide (3g)**: Light brown solid; Yield: 44.6%; m.p.: 141.2–143.6 °C; ^{1}H NMR (400 MHz, [D$_6$]DMSO): δ = 8.75 (s, 1H), 8.13 (ddd, J_1 = 7.3 Hz, J_2 = 5.0 Hz, J_3 = 1.5 Hz, 1H), 7.93 (dd, J_1 = 4.9 Hz, J_1 = 1.4 Hz, 1H), 7.54 (t, J = 7.7 Hz, 1H), 7.50 (d, J = 7.5 Hz, 1H), 7.32 (d, J = 1.4 Hz, 1H), 7.04 (dd, J_1 = 7.5 Hz, J_2 = 1.4 Hz, 1H), 4.80 (s, 2H); ^{13}C NMR (400 MHz, [D$_6$] DMSO): δ = 166.58, 159.63, 157.12, 135.54, 131.53, 130.97, 127.19, 127.11, 123.71, 117.19, 116.98, 116.96, 113.85, 99.93, 67.31.

***N*-(3-Cyano-4-fluorophenyl)-2-[(quinolin-8-yl)oxy]acetamide (3h)**: Brown solid; Yield: 87.0%; m.p.: 130.1–132.4 °C; ^{1}H NMR (400 MHz, [D$_6$]DMSO): δ = 10.94 (s, 1H), 8.96 (dd, J_1 = 7.5 Hz, J_2 = 1.4 Hz, 1H), 8.01–7.98 (m, 1H), 7.96 (dd, J_1 = 3.1, J_2 = 1.7 Hz, 1H), 7.95 (dd, J_1 = 4.9 Hz, J_2 = 1.4 Hz, 1H), 7.62 (t, J = 8.2 Hz, 1H), 7.55–7.53 (m, 1H), 7.51 (dt, J_1 = 7.5 Hz, J_2 = 1.5 Hz, 1H), 7.33 (d, J = 7.5 Hz, 1H), 7.29 (t, J = 7.7 Hz 1H), 4.99 (s, 1H); ^{13}C NMR (400 MHz, [D$_6$]DMSO): δ = 167.93, 159.65, 157.19, 149.45, 149.87,121.44, 136.23, 135.49, 129.20, 126.93, 123.38, 122.09, 121.44, 117.31, 117.11, 113.30, 100.03, 69.57.

2-[(5-Chloroquinolin-8-yl)oxy]-*N*-(3-cyano-4-fluorophenyl) acetamide (3i): Dark yellow solid; Yield: 80.0%; m.p.: 163.8–165.9 °C; ^{1}H NMR (400 MHz, [D$_6$]DMSO): δ = 10.74 (s, 1H), 9.02 (dd, J_1 = 4.1 Hz, J_2 = 1.5 Hz, 1H), 8.53 (dd, J_1 = 8.6 Hz, J_2 = 1.5 Hz, 1H), 8.03 (dd, J_1 = 4.9 Hz, J_2 = 1.4 Hz, 1H), 7.90-7.87 (m, 1H), 7.52 (t, J = 7.8 Hz, 2H); 7.50 (t, J = 9.1 Hz, 1H), 7.31–7.29 (m, 1H), 6.17 (d, J = 8.4 Hz, 1H), 4.98 (s, 1H), ^{13}C NMR (400 MHz, [D$_6$]DMSO): δ = 168.59, 167.27, 153.77, 150.60, 135.88, 132.92, 127.37, 127.25, 125.82, 126.72, 123.82, 123.71, 117.70, 116.56, 112.02, 95.03, 69.07.

General procedure for the preparation of compounds (4a–4i): A mixture of compounds **3a-3i** (3.20 to 4.69 mmol), guanidine carbonate (8.8 to 11.7 mmol) and 50% (*w/v*) of diisopropylethylamine (DIPEA) were dissolved in DMF anhydrous in a vial. The reaction was submitted to successive 20 min periods of microwave irradiation of 850 W of power, in which total irradiation time was carried out in 1.5 to 2.5 h, with a final temperature of 145 °C. This latter was monitored with TLC, upon completion the reaction mixture was poured into ice-water, the solid was filtered. Afterwards the solid was isolated as described previously.

***N*-(2,4-diaminoquinazolin-6-yl)-2-phenoxyacetamide (4a)**: Light brown solid; Yield: 23.7%; m.p.: 153.7–155.3 °C; ^{1}H NMR (400 MHz, [D$_6$]DMSO): δ = 10.45 (s, 1H), 8.17 (s, 2H), 8.15 (dd, J = 5.8, 2.7 Hz, 1H), 8.11 (d, J = 7.7 Hz, 1H), 7.98 (s, 2H), 7.97 (d, J = 2.1 Hz, 1H), 7.95 (d, J = 2.1 Hz, 1H), 7.52 (t, J = 9.1 Hz, 2H), 7.05–6.95 (m, 2H), 4.72 (s, 2H); ^{13}C NMR (400 MHz, [D$_6$]DMSO): δ = 167.36, 159.74, 157.76, 157.19, 135.59, 129.66, 127.22, 123.79, 121.44, 117.73, 114.81, 113.95, 99.93, 67.08; HRMS (APCI+) *m/z* calcd for $C_{16}H_{15}N_5O_2$ $[M+H]^+$: 310.1298, found: 310.1202.

***N*-(2,4-diaminoquinazolin-6-yl)-2-(3-methoxyphenoxy)acetamide (4b)**: Brown solid; Yield: 28.7%; m.p.: 301.9–302.9 °C; ^{1}H NMR (400 MHz, [D$_6$]DMSO): δ = 9.97 (s, 1H), 8.09 (s, 2H), 8.08 (d, J = 2.2 Hz, 1H), 7.58 (dd, J_1 = 8.9 Hz, J_2 = 2.3 Hz, 1H), 7.57 (s, 2H), 7.46 (d, J = 8.7 Hz, 1H), 7.45 (t, J = 7.5 Hz, 1H), 6.61 (dt, J_1 = 7.5 Hz, J_2 = 1.4 Hz, 1H), 6.58 (dt, J_1 = 7.5 Hz, J_2 = 1.4 Hz, 1H), 6.57–6.58 (m, 1H), 5.93 (s, 2H), 4.67 (s, 3H); ^{13}C NMR (400 MHz, [D$_6$]DMSO): δ = 166.24, 162.33, 160.40, 160.20, 159.01, 149.49, 130.79, 130.01, 127.77, 124.34, 115.36, 109.82, 106.90, 106.80, 101.18, 67.20, 55.53; HRMS (APCI+) *m/z* calcd for $C_{17}H_{17}N_5O_3$ $[M+H]^+$: 340.1404, found: 340.1274.

2-(3-Acetamidophenoxy)-*N*-(2,4-diaminoquinazolin-6-yl) acetamide (4c): Light brown solid; Yield: 31.5%; m.p.: 139.3–140.8 °C; ^{1}H NMR (400 MHz, [D$_6$]DMSO): δ = 10.19 (s, 1H), 10.06 (s, 1H), 8.19 (s, 2H), 8.18 (d, J = 7.5 Hz, 1H), 7.67 (dd, J_1 = 7.5 Hz, J_2 = 1.4 Hz, 1H), 7.67 (s, 2H), 7.42 (d, J = 1.4 Hz, 1H), 7.26(t, J = 3.9 Hz, 1H), 7.31–7.21 (m, 1H), 7.19 (t, J = 7.6 Hz, 1H), 6.68 (dd, J_1 = 8.0 Hz, J_2 = 1.5 Hz, 1H), 4.67 (s, 2H), 2.04 (s, 3H); ^{13}C NMR (400 MHz, [D$_6$]DMSO): δ = 178.92, 177.28, 168.27, 166.36, 158.83, 158.11, 154.87, 140.48, 131.24, 129.45, 128.13, 122.62, 112.13, 109.73, 108.84, 108.64, 67.06, 23.97; HRMS (APCI+) *m/z* calcd for $C_{18}H_{18}N_6O_3$ $[M+H]^+$: 367.1531, found: 367.1356.

***N*-(2,4-Diaminoquinazolin-6-yl)-2-(3-methylphenoxy)acetamide (4d)**: Cream solid; Yield: 43.5%; m.p.: 134.7–136.3 °C; ^{1}H NMR (400 MHz, [D$_6$]DMSO): δ = 10.44 (s, 1H), 7.74 (s, 2H), 7.73 (dd, J_1 = 9.1 Hz, J_2 = 2.6 Hz, 1H), 7.52 (d, J = 9.1 Hz, 1H), 7.32 (d, J = 2.6 Hz, 1H), 7.26 (t, J = 7.8 Hz, 1H), 7.17 (s, 2H), 7.23 (t, J = 1.5 Hz, 1H), 7.97 (dt, J_1 = 4.5 Hz, J_2 = 3.6 Hz, 1H), 7.21 (dt, J_1 = 4.6 Hz, J_2 = 3.7 Hz, 1H), 4.70 (s, 2H), 2.28 (s, 3H); ^{13}C NMR (400 MHz, [D$_6$]DMSO): δ = 167.29, 159.67, 157.66, 157.16, 135.51, 129.59, 127.23, 127.15, 121.37, 117.25, 117.05, 116.96, 114.74, 113.93, 99.95, 67.01, 21.08; HRMS (APCI+) *m/z* calcd for $C_{17}H_{17}N_5O_2$ $[M+H]^+$: 324.1455, found: 324.1348.

2-(3-Chlorophenoxy)-*N*-(2,4-diaminoquinazolin-6-yl)acetamide (4e): Brown solid; Yield: 37.5%; m.p.: 239.8–240.7 °C; ^{1}H NMR (400 MHz, [D$_6$]DMSO): δ = 10.05 (s, 1H), 8.11 (d, J = 8.8 Hz, 1H), 7.95 (s, 2H),), 7.58 (dd, J_1 = 8.9 Hz, J_2 = 2.2 Hz, 1H), 7.37 (s, 2H), 7.35 (t, J = 8.2 Hz, 1H), 7.20 (d, J = 2.2 Hz, 1H), 7.13 (t, J = 2.2 Hz, 1H), 7.06–7.04 (m, 1H), 7.03–7.02 (m, 1H), 4.75 (s, 2H) ^{13}C NMR (400 MHz, [D$_6$] DMSO): δ = 176.55, 170.60, 161.81, 160.02, 159.08, 133.62, 130.97, 130.37, 128.42, 124.06, 121.19, 115.37, 115.05, 113.73, 109.83, 67.30; HRMS (APCI+) *m/z* calcd for $C_{16}H_{14}ClN_5O_2$ $[M+H]^+$: 344.0908, found: 344.0791.

***N*-(2,4-Diaminoquinazolin-6-yl)-2-(3-nitrophenoxy)acetamide (4f)**: Yellow solid; Yield: 40.2%; m.p.: 178.2–179.9 °C; ^{1}H NMR (400 MHz, [D$_6$]DMSO): δ = 8.97 (s, 1H), 7.78 (s, 2H), 7.74 (d, J = 4.1 Hz, 1H), 7.78–7.77 (m, 1H), 7.66 (s, 2H), 7.58 (dd, J_1 = 7.5 Hz, J_2 = 1.8 Hz, 1H), 7.57 (d, J = 8.1 Hz, 1H), 7.52 (t, J = 8.6 Hz, 1H), 7.48 (d, J = 1.8 Hz, 1H), 7.46–7.45 (m, 1H), 3.35 (s, 2H); ^{13}C NMR (400 MHz, [D$_6$]DMSO): δ = 182.22, 159.38, 156.08, 149.23, 144.71, 139.65, 131.17, 126.13, 122.46, 122.04, 118.15, 114.87, 114.46, 110.36, 100.74, 74.99; (APCI+) *m/z* calcd for $C_{16}H_{14}N_6O_4$ $[M+H]^+$: 355.1149, found: 355.2793.

***N*-(2,4-Diaminoquinazolin-6-yl)-2-(3,4-dichlorophenoxy)acetamide (4g)**: Light brown solid; Yield: 38.4%; m.p.: 122.3–124.8 °C; ^{1}H NMR (400 MHz, [D$_6$]DMSO): × × δ = 8.80 (s, 1H), 8.60 (s, 2H), 8.26 (s, 2H), 7.87 (d, J = 9.8 Hz, 1H), 7.69 (dd, J_1 = 9.8 Hz, J_2 = 2.7 Hz, 1H), 7.34 (s, 2H), 7.21 (d, J = 2.7 Hz, 1H), 7.14 (d, J = 8.8 Hz, 1H), 7.05 (d, J = 2.7 Hz, 1H), 6.98 (dd, J_1 = 8.8 Hz, J_2 = 2.7 Hz, 1H), 3.35 (s, 2H); ^{13}C NMR (400 MHz, [D$_6$]DMSO): δ = 170.07, 148.56, 139.44, 131.72, 130.95, 128.67, 125.38, 125.20, 119.70, 117.62, 116.51, 116.11, 114.27, 112.57, 110.13, 67.42; HRMS (APCI+) *m/z* calcd for $C_{16}H_{13}Cl_2N_5O_2$ $[M+H]^+$: 378.0519, found: 378.0523.

***N*-(2,4-Diaminoquinazolin-6-yl)-2-[(quinolin-8-yl)oxy]acetamide (4h)**: Cream solid; Yield: 41.0%; m.p.: 173.8–174.5 °C; ^{1}H NMR (400 MHz, [D$_6$]DMSO): δ = 10.90 (s, 1H), 8.97 (s, 2H), 8.96 (dd, J_1 = 4.2 Hz, J_2 = 1.7 Hz, 1H), 8.38 (dd, J_1 = 7.77 Hz, J_2 = 1.7 Hz, 1H), 7.97 (ddd, J_1 = 9.2 Hz, J_2 = 4.8 Hz, J_3 = 2.8 Hz, 1H), 7.96 (s, 2H), 7.95 (dd, J_1 = 7.5 Hz, J_2 = 1.6 Hz, 1H), 7.65 (dd, J_1 = 8.4 Hz, J_2 = 1.2 Hz, 1H), 7.62 (d, J = 1.4 Hz, 1H), 7.61–7.59 (m, 1H), 7.55–7.51 (m, 1H), 7.34 (dd, J_1 = 8.3 Hz, J_2 = 1.1 Hz, 1H), 4.99 (s, 2H); ^{13}C NMR (400 MHz, [D$_6$] DMSO): δ = 168.26, 158.19, 155.76, 153.36, 148.17, 139.63, 138.90, 138.71, 136.18, 128.66, 127.14, 126.2, 122.29, 118.23, 117.21, 114.19, 109.46, 100.27, 68.23; HRMS (APCI+) *m/z* calcd for $C_{19}H_{16}N_6O_2$ $[M+H]^+$: 361.1407, found: 361.2459.

2-[(5-Chloroquinolin-8-yl)oxy]-*N*-(2,4-diaminoquinazolin-6-yl) acetamide (4i): Light yellow solid; Yield: 36.7%; m.p.: 165.0–166.8 °C; ^{1}H NMR (400 MHz, [D$_6$]DMSO): δ = 9.05 (s, 1H), 8.97 (s, 2H), 8.96 (dd, J_1 = 4.2 Hz, J_2 = 1.6 Hz, 1H), 8.51 (dd, J_1 = 4.5 Hz, J_2 = 1.6 Hz, 1H), 8.50 (s, 2H), 7.85 (dd, J_1 = 8.5 Hz, J_2 = 2.8 Hz, 1H), 7.58 (d, J = 8.4 Hz, 1H), 7.08 (d, J = 7.8 Hz, 1H), 7.78 (d, J = 4.1 Hz, 1H), 7.47 (t, J = 9.1 Hz, 1H), 7.08 (d, J = 8.3 Hz, 1H), 3.33 (s, 2H); ^{13}C NMR (400 MHz, [D$_6$]DMSO): δ = 177.99, 159.08, 155.67, 148.95, 148.62, 138.97, 132.60, 132.44, 132.52, 127.40, 127.16, 127.05, 125.96, 123.31, 118.66, 117.30, 114.11, 109.05, 79.67; HRMS (APCI+) *m/z* calcd for $C_{19}H_{15}ClN_5O_2$ $[M+H]^+$: 395.1017, found: 395.1703.

Antiproliferative activity assay

Quinazoline derivatives were tested *in vitro* for their antiproliferative activity in five different human cancer cell lines representative of prostate cancer (PC-3), colon cancer (HCT-15), breast cancer (MCF-7), double-negative breast cancer (MDA-MB-231), and lung cancer (SK-LU-1) and noncancerous monkey's kidney cells (COS-7) and peripheral blood mononuclear cells (PBMC). PBMC were obtained from human blood samples with informed and signed consent, and insolated using the Ficoll-Paque method (GE Healthcare ®) reported by Jia et al. Cancerous and COS-7 cell lines were acquired from the American Type Culture Collection (ATCC). Cell lines were cultured in RPMI-1640 containing 10% fetal bovine serum (FBS), 1% of a mix of antibiotic and antifungal, under humified atmosphere of 5% CO_2 at 37 °C. Cells were detached from a sub-confluent culture in T25 flasks with a PBS-EDTA solution and seeded (2×10^4 cells/well) in 96-well plates. Compounds were used at 25 μM and incubated at 37 °C for 48 h. The assays were stopped by the addition of 50 μL of 5% (*w/v*) cold trichloroacetic acid (TCA) an incubated at 4 °C for 1 h. The supernatant was discarded and afterwards the plate was washed with tap water, letting it be air dried. Then, sulforhodamine B (SRB) cell proliferation assay was employed to estimate cell viability (these was done thrice for each compound). For this, cells were incubated with 0.4% of SRB solution for 0.5 h at RT. Unbound SRB was washed away with an acetic acid solution at 1%, allowing the plates to dry at RT. Samples were dissolved with 100 μL of Tris buffer at pH 10.5 for 10 min. The optical density was determined at 490 nm with a microplate reader DAIGGER (BioTek ®). The percent of growth inhibition was calculated based on the control sample (cells treated with 0.01% DMSO). Dose-response curves were performed with compounds that exhibited the best activity against MDA-MB-231 and SK-LU-1 cells. The sensitivity towards cancer cell lines was reported in a half inhibitory concentration values (IC_{50}), which are means ± SD of three independent experiments at a concentration range of 0.00125 μM to 80 μM.

Indirect immunofluorescence assays

SK-LU-1 cells ($4\times x\ 10^5$) were seeded on coated glass slides (Sigma-Aldrich) and incubated in DMEM for 24 h with compounds **4d** (25.0 μM), **4e** (12.5 μM), and **4i** (2.5 and 5.0 μM). DMSO (0.01%) was included as negative control and PTX (0.08 μM), NZ (0.16 μM) and COL (0.30 μM) as positive controls. Afterwards, cells were fixed in 4% of paraformaldehyde in phosphate-buffered saline 1X (PBS) pH 7.4 for 1 h at 4 °C. Nonspecific binding was blocked with 1% bovine serum albumin (BSA) in PBS for 1 h at 37 °C. After this, treated cells were incubated for 1 h at RT with a monoclonal antibody anti-β-tubulin (Aldrich ® T0198) diluted 1:1000; subsequently the secondary antibody, anti-mouse-FITC (Millipore ® AP308F; 1:500 dilution), containing 4′,6′-diamidino-2-phenylindole (DAPI) at 1:1000 dilution was incubated for 1 h at RT. The cover slips were washed three times with PBS and mounted on glass slides with Vectashield (Vector Laboratories). Images were acquired on a Nikon Ti Eclipse ® inverted confocal microscope equipped with an A1 imaging system. Imaging was performed using a 20× (dry, NA 0.8) objective lens. Dyes were excited in a sequential mode using the built-in laser lines: 403 nm (DAPI), 488 nm (FITC). Corresponding emissions were read in the following ranges: 425–475 nm (DAPI) and 500–550 nm (FITC), using the manufacturer-provided filter sets.

Western blot analysis of soluble and polymerized tubulin

SK-LU-1 cells (1.65×10^6 cells) cultured in D-MEM medium complemented with FBS (10%) were seeded in 60 mm petri dishes and treated with compounds **4e** and **4i** and reference drugs at different concentrations for 24 h at 37 °C. Then, cells were washed with PBS 1× and permeabilized with two different buffers to obtain soluble and polymerized tubulin as previously recommended.[37] To collect soluble fraction, cells were permeabilized with 1000 μL lysis buffer [80 mM Pipes-KOH (pH 6.8) 1 mM $MgCl_2$, 1 mM EGTA, 02% Triton X-100, 10% glycerol, 0.1% protease inhibitor cocktail (Sigma ®)] for 3 min at 30 °C. Afterwards, soluble tubulin contained in lysis buffer was gently removed. Polymerized tubulin (insoluble fraction)) was obtained with 1000 μL of Laemmli's buffer [180 mM, Tris-HCl (pH 6.8), 6% SDS, 15% glycerol, 7.5% β-mercaptoethanol and 0.01% of Bromophenol Blue] which was heated for 3 min at 95 °C. Quantification of all samples was carried out twice for each sample with the 2D Quant kit (GE Healthcare ®). Soluble and polymerized tubulin (30 μg) were run on SDS-12% polyacrylamide gel for 1 h 30 min at 100 V and transferred to a nitrocellulose membrane (Biorad®). Membrane was incubated with a monoclonal antibody anti-beta-tubulin (Sigma-Aldrich) at 1:1000 dilution for 1 h 30 min at 37 °C. After this, membrane was washed 3× with PBS 1× and incubated with the goat anti-mouse IgG1 secondary antibody horseradish peroxidase conjugated (HRP, Millipore ® AP308P) (1:1000 dilution) for 1 h 30 min at 37 °C. Bands were revealed with a chromogenic solution [30% of H_2O_2 solution, 4-chloro-1-naphthol and triethylamine buffer].

Images were captured with a photodocumenter (UVITEC Cambridge) and intensity of each band was analyzed with Quantity One 4.6 software (Biorad ®).

Tubulin polymerization inhibition

The *in vitro* tubulin polymerization assays were performed using the kit (cat. # BK006P) manufactured by Cytoskeleton Inc., Denver, CO, USA. Assays were carried following the instructions provided by the manufacturer.[38,39] Cold purified porcine neural tubulin protein (>99% purity) was suspended in G-PEM buffer (80 mM PIPES, 2 mM $MgCl_2$, 0.5 mM EGTA, 1 mM GTP, pH 6.9) containing 10% glycerol in the absence or presence of the compounds at 4 °C. Quinazoline derivatives **4e** (10 μM), **4i** (10 μM, 5 μM and 2.5 μM) and the reference compounds, PTX (10 μM) and NZ (0.16 μM), were tested in duplicate. Tubulin polymerization was measured by an increase in absorbance at 340 nm over a period of 50 min at 37 °C in a BioTek Epoch™ Microplate Spectrophotometer.

Computational studies

pK_a calculation. Chemicalize tool (https://chemicalize.com/, RA-O Academic License), developed by ChemAxon (http://www.chemaxon.com),[40,41] was used to predict the pK_a and assign N1 nitrogen protonation state of compounds **4e** ($pK_{aN1} = 6.98$) and **4i** ($pK_{a\,N1} = 6.98$).

Heterodimer model preparation. The X-ray crystal structures of the α-tubulin (PDB ID: 5YL2,[42] chain C) and β-tubulin (PDB ID: 5CA1,[12] chain D) were retrieved from the PDB.[43] Both model structures were completed with SwissModel server.[44] The α/β-tubulin heterodimer was assembled in PyMOL v1.7[45] employing PDB ID: 5CA1 as a template. Based on our previous study, Glu198 residue was fixed in the protonated state.[15] The heterodimer structure was further submitted to a mild energy minimization using CHARMM36[46] force field implemented in GROMACS v5.1.4.[47] Finally, we employed the MGLTools 1.5.4[48] graphic interface to assign partial charges to the atoms with the Gasteiger-Marsili method, merge the nonpolar hydrogens, and save the structure into a PDBQT coordinate file.

Ligand preparation. The 3D structures of compounds **4e** and **4i** were energy minimized using the MMFF94 s force field imple-

mented in the *obminimize* module of OpenBabel toolbox.[49] Subsequently, we assigned the rotatable bonds, atom partial charges, and saved each PDBQT file using MGLTools 1.5.4.

Protein-ligand docking. Compounds **4e** and **4i** were docked in the NZ/COL binding site employing AutoDock 4.2.6 software.[48] A grid box of $80\times80\times80$ points with a spacing of 0.375 Å was centered in the binding site. A total of 50 runs were performed using the Lamarckian generic algorithm as search method, 2.5×10^6 energy evaluations and an initial population of 150 conformers.

Molecular dynamics simulations. The α/β-tubulin heterodimers complexed with compounds **4e** and **4i** were submitted to MD simulations using the AMBER99SB-ILDN force field[50] implemented in the GROMACS 5.1.4 package.[47] ACPYPE interface[51] was used to set up the topologies of GTP and the quinazoline derivatives, computing the AM1-BCC charges. Each complex was energy minimized employing the *steepest descent* algorithm and equilibrated under standardized NVT and NPT conditions ($T=300$ K and $P=1.0$ bar). V-rescale[52] coupling thermostat and Parrinello-Rahman[53] algorithms were employed during the equilibration and production runs. Nonpolar hydrogens were constrained using the LINCS algorithm.[54] The Lennard-Jones potential and short-range electrostatic interactions were computed within a cutoff radius of 1.0 nm. PME method was used to calculate the long-range electrostatic interactions. Each system was submitted to 100 ns MD production run using 2-fs as time step. The root-mean-square deviation (RMSD), root-mean-square fluctuations (RMSF), hydrogen bonds (HBs), and number of contacts (cutoff value of 3.5 Å) were computed using built-in tools of the GROMACS 5.1.4 package.

Acknowledgements

F.S.H.-V. (no. 629489) and R.A.-O. (no. 288862) are very grateful to CONACyT for the scholarships granted. The authors thank Dr. Vadim Pérez Koldenkova from the Laboratorio Nacional de Microscopia Avanzada, Centro Médico Nacional Siglo XXI, IMSS for his technical support in confocal microscopy. We thank Ana Rosa Duarte and Erica Burgeño-Bucio from the Unidad de Investigación Preclínica (UNIPREC) for their technical support in PBMC assays. We also thank Dr. Jaime Pérez-Villanueva from the Universidad Autónoma Metropolitana, Unidad Xochimilco (UAM-X) for his technical support in absorbance spectrophotometry experiments. L.D. thanks the Dirección General de Cómputo y de Tecnologías de Información y Comunicación for the support received in the use of the HP Cluster Platform 3000SL supercomputer "Miztli" (LANCAD-UNAM-DGTIC-306). This study was sponsored by grants from UNAM-DGAPA-PAPIIT IN218117, CONACYT-CB220664, and CONACYT-CB (A1-S-8866).

Conflict of Interest

The authors declare no conflict of interest.

Keywords: antiproliferative activity · diaminoquinazoline · molecular dynamics · nocodazole site · tubulin polymerization inhibition

[1] C. P. Garnham, A. Roll-Mecak, *Cytoskeleton* **2012**, *69*, 442–463.
[2] K. J. Mickolajczyk, E. A. Geyer, T. Kim, L. M. Rice, W. O. Hancock, *Proc. Natl. Acad. Sci. USA* **2019**, *116*, 7314–7322.
[3] M. A. Jordan, L. Wilson, *Nat. Rev. Cancer* **2004**, *4*, 253–265.
[4] A. L. Parker, M. Kavallaris, J. A. McCarroll, *Front. Oncol.* **2014**, *4*, 153.
[5] B. P. Chatterji, B. Jindal, S. Srivastava, D. Panda, *Expert Opin. Ther. Pat.* **2011**, *21*, 167–186.
[6] M. Salama, A. Shalash, A. Magdy, M. Makar, T. Roushdy, M. Elbalkimy, H. Elrassas, P. Elkafrawy, W. Mohamed, M. B. Abou Donia, *PLoS One* **2018**, *13*, 1–11.
[7] H. Guo, X. Li, Y. Guo, L. Zhen, *Med. Chem. Res.* **2019**, *28*, 927–937.
[8] M. O. Steinmetz, A. E. Prota, *Trends Cell Biol.* **2018**, *28*, 776–792.
[9] Y. Lu, J. Chen, M. Xiao, W. Li, D. D. Miller, *Pharm. Res.* **2012**, *29*, 2943–2971.
[10] B. Gigant, A. Cormier, A. Dorléans, R. B. G. Ravelli, M. Knossow, in *Tubulin-Binding Agents Synth. Struct. Mech. Insights* (Ed.: T. Carlomagno), Springer, Berlin, **2009**, pp. 259–278.
[11] P. Barbier, A. Dorle, F. Devred, L. Sanz, D. Allegro, C. Alfonso, M. Knossow, V. Peyrot, J. M. Andreu, G. Yvette, et al., *J. Biol. Chem.* **2010**, *285*, 31672–31681.
[12] Y. Wang, H. Zhang, B. Gigant, Y. Yu, Y. Wu, X. Chen, Q. Lai, Z. Yang, Q. Chen, J. Yang, *FEBS J.* **2016**, *283*, 102–111.
[13] R. Aguayo-Ortiz, L. Cano-González, R. Castillo, A. Hernández-Campos, L. Dominguez, *Chem. Biol. Drug Des.* **2017**, *90*, 40–51.
[14] S. Majumdar, S. Maiti, S. Ghosh Dastidar, *Biochemistry* **2016**, *55*, 335–347.
[15] D. C. Guzmán-Ocampo, R. Aguayo-Ortiz, L. Cano-González, R. Castillo, A. Hernández-Campos, L. Dominguez, *ChemMedChem* **2018**, *13*, 20–24.
[16] A. E. Prota, F. Danel, F. Bachmann, K. Bargsten, R. M. Buey, J. Pohlmann, S. Reinelt, H. Lane, M. O. Steinmetz, *J. Mol. Biol.* **2014**, *426*, 1848–1860.
[17] M. Kamel, W. Zaghary, R. Al-Wabli, M. Anwar, *Egypt. Pharm. J.* **2016**, *15*, 98.
[18] F. S. Herrera-Vázquez, F. Hernández-Luis, J. L. Medina Franco, *Med. Chem. Res.* **2019**, *28*, 395–416.
[19] Shagufta, I. Ahmad, *MedChemComm* **2017**, *8*, 871–885.
[20] A. S. Matus-Meza, M. A. Velasco-Velázquez, F. Hernández-Luis, *Med. Chem. Res.* **2018**, *27*, 1748–1756.
[21] B. Roth, J. Z. Strelitz, *J. Org. Chem.* **1969**, *34*, 821–836.
[22] N. Srimongkolpithak, S. Sundriyal, F. Li, M. Vedadi, M. J. Fuchter, *MedChemComm* **2014**, *5*, 1821–1828.
[23] J. P. Santa Maria, Y. Park, L. Yang, N. Murgolo, M. D. Altman, P. Zuck, G. Adam, C. Chamberlin, P. Saradjian, P. Dandliker, et al., *ACS Chem. Biol.* **2017**, *12*, 2448–2456.
[24] S. Majumdar, D. Basu, S. Ghosh Dastidar, *J. Chem. Inf. Model.* **2019**, *59*, 2274–2286.
[25] K. Upadhyaya, Hamidullah, K. Singh, A. Arun, M. Shukla, N. Srivastava, R. Ashraf, A. Sharma, R. Mahar, S. K. Shukla, et al., *Org. Biomol. Chem.* **2016**, *14*, 1338–1358.
[26] L. Niu, J. Yang, W. Yan, Y. Yu, Y. Zheng, H. Ye, Q. Chen, L. Chen, *J. Biol. Chem.* **2019**, 294, 18099–18108..
[27] M. H. Cohen, G. A. Williams, R. Sridhara, G. Chen, R. Pazdur, *Oncologist* **2003**, *8*, 303–306.
[28] I. Leizerman, R. Avunie-Masala, M. Elkabets, A. Fich, L. Gheber, *Cell. Mol. Life Sci.* **2004**, *61*, 2060–2070.
[29] E. Romano, M. V. Castillo, J. L. Pergomet, J. Zinczuk, S. A. Brandán, *Open J. Synth. Theory Appl.* **2013**, *02*, 8–32.
[30] R. Romagnoli, P. G. Baraldi, A. Brancale, A. Ricci, E. Hamel, R. Bortolozzi, G. Basso, G. Viola, *J. Med. Chem.* **2011**, *54*, 5144–5153.
[31] S. M. Devine, C. Yong, D. Amenuvegbe, L. Aurelio, D. Muthiah, C. Pouton, R. Callaghan, B. Capuano, P. J. Scammells, *J. Med. Chem.* **2018**, *61*, 8444–8456.
[32] L. J. Leandro-García, S. Leskelä, I. Landa, C. Montero-Conde, E. López-Jiménez, R. León, A. Cascón, M. Robledo, C. Rodríguez-Antona, *Cytoskeleton.* **2010**, *67*, 214–223.
[33] C. Yong, S. M. Devine, X. Gao, A. Yan, R. Callaghan, B. Capuano, P. J. Scammells, *ChemMedChem* **2019**, *14*, 1968–1981.
[34] J. Yang, W. Yan, Y. Li, L. Niu, H. Ye, L. Chen, *Mol. Pharmacol.* **2019**, *96*, 711–719.
[35] C. R. Yang, B. Peng, S. L. Cao, T. T. Ren, W. Jiang, F. C. Wang, Y. S. Li, G. Wang, Z. Li, S. Xu, et al., *Eur. J. Med. Chem.* **2018**, *154*, 324–340.
[36] J. Yang, W. Yan, Y. Yu, Y. Wang, T. Yang, L. Xue, X. Yuan, C. Long, Z. Liu, X. Chen, et al., *J. Biol. Chem.* **2018**, *293*, 9461–9472.
[37] A. Kamal, A. B. Shaik, S. Polepalli, V. S. Reddy, G. B. Kumar, S. Gupta, K. V. S. R. Krishna, A. Nagabhushana, R. K. Mishra, N. Jain, *Org. Biomol. Chem.* **2014**, *12*, 7993–8007.

[38] M. L. Shelanski, F. Gaskin, C. R. Cantor, *Proc. Natl. Acad. Sci. USA* **1973**, *70*, 765–768.
[39] J. C. Lee, S. N. Timasheff, *Biochemistry* **1977**, *16*, 1754–1764.
[40] C. Ltd., *J. Chem. Inf. Model.* **2012**, *52*, 613–615.
[41] H. E. Pence, A. Williams, *J. Chem. Educ.* **2010**, *87*, 1123–1124.
[42] K. Sakchaisri, S. O. Kim, J. Hwang, N. K. Soung, K. H. Lee, T. W. Choi, Y. Lee, C. M. Park, N. R. Thimmegowda, P. Y. Lee, et al., *PLoS One* **2017**, *12*, 1–18.
[43] H. M. Berman, J. Wstbrook, Z. Feng, G. Gilliland, T. N. Bhat, H. Weissing, I. N. Shindyalov, P. E. Bourne, *Nucleic Acids Res.* **2000**, *28*, 235–242.
[44] M. Biasini, S. Bienert, A. Waterhouse, K. Arnold, G. Studer, T. Schmidt, F. Kiefer, T. G. Cassarino, M. Bertoni, L. Bordoli, et al., *Nucleic Acids Res.* **2014**, *42*, 252–258.
[45] L. Schrödinger, *The PyMOL Molecular Graphics System*, *Version 1.7 Schrödinger*, *LLC.*, **2015**.
[46] J. Huang, A. D. M. Jr, *J. Comput. Chem.* **2013**, *34*, 2135–2145.
[47] M. J. Abraham, T. Murtola, R. Schulz, S. Páall, J. C. Smith, B. Hess, E. Lindah, *SoftwareX* **2015**, *1–2*, 19–25.
[48] G. M. Morris, R. Huey, W. Lindstrom, M. F. Sanner, R. K. Belew, D. S. Goodsell, A. J. Olson, *J. Comput. Chem.* **2009**, *30*, 2785–2791.
[49] N. M. O'Boyle, M. Banck, C. A. James, C. Morley, T. Vandermeersch, G. R. Hutchison, *J. Cheminf.* **2011**, *3*, 1–14.
[50] K. Lindorff-Larsen, S. Piana, K. Palmo, P. Maragakis, J. L. Klepeis, R. O. Dror, D. E. Shaw, *Proteins Struct. Funct. Bioinf.* **2010**, *78*, 1950–1958.
[51] A. W. Sousa da Silva, W. F. Vranken, *BMC Res. Notes* **2012**, *5*, 367.
[52] G. Bussi, D. Donadio, M. Parrinello, *J. Chem. Phys.* **2007**, *126*, 014101.
[53] M. Parrinello, A. Rahman, *J. Chem. Phys.* **1982**, *76*, 2662–2666.
[54] B. Hess, H. Bekker, H. J. C. Berendsen, J. G. E. M. Fraaije, *J. Comput. Chem.* **1997**, *18*, 1463–1472.
[55] F.-Y. Lin, A. D. MacKerell, *J. Phys. Chem. B* ***2017***, *121*, 6813–6821.
[56] Y. Jia, H. Xu, Y. Li, C. Wei, R. Guo, F. Wang, Y. Wu, J. Liu, J. Jia, J. Yan, et al., *Biopreserv. Biobank.* **2018**, *16*, 82–91.

Manuscript received: March 24, 2020
Revised manuscript received: June 4, 2020
Accepted manuscript online: July 19, 2020
Version of record online: August 26, 2020